

## Electronic Supplementary Information

---

### **Carbon coated nickel phosphides porous nanoplates for highly efficient oxygen evolution reaction**

*Xin-Yao Yu,<sup>a b c</sup> Yi Feng,<sup>a</sup> Buyuan Guan,<sup>b</sup> Xiong Wen (David) Lou<sup>\*b</sup> and U. Paik<sup>\*a</sup>*

<sup>a</sup> WCU Department of Energy Engineering, Hanyang University, Seoul 133-791, Korea

Email: [upaik@hanyang.ac.kr](mailto:upaik@hanyang.ac.kr)

<sup>b</sup> School of Chemical and Biomedical Engineering, Nanyang Technological University, 62 Nanyang Drive, Singapore 637459 E-mail: [xwlou@ntu.edu.sg](mailto:xwlou@ntu.edu.sg)

<sup>c</sup> Hefei Institutes of Physical Science, Chinese Academy of Sciences, Hefei 230031, PR China

## Experimental details

*Synthesis of Ni-Ni PBA nanoplates.* The Ni-Ni PBA nanoplates were synthesized by a simple precipitation method. In a typical procedure, 95 mg of  $\text{NiCl}_2 \cdot x\text{H}_2\text{O}$  and 88 mg of sodium citrate were dissolved in 20 mL of deionized (DI) water to form solution A. 96 mg of potassium tetracyanonickelate(II) was dissolved in 20 mL of DI water to form solution B. Then, solutions A and B were mixed under magnetic stirring for 3 min. The obtained mixed solution was aged for 12 h at room temperature. After collected by centrifugation and washed with water and ethanol, the precipitates were dried at 70 °C overnight.

*Synthesis of Ni-P porous nanoplates.* In a typical synthesis of Ni-P nanoplates, the obtained Ni-Ni PBA nanoplates were phosphidated by thermal decomposition of  $\text{NaH}_2\text{PO}_2$  under Ar flow. 20 mg of Ni-Ni PB analogues nanoplates and 200 mg of  $\text{NaH}_2\text{PO}_2$  were put at two separate positions in a porcelain boat with  $\text{NaH}_2\text{PO}_2$  at the upstream side of the tube furnace. Then, the samples were annealed at 300 °C for 2 h with a heating rate of 3 °C  $\text{min}^{-1}$  under Ar atmosphere with a flow rate of 60 sccm. The Ni-P nanoplates were obtained after cooling to ambient temperature under Ar.

*Synthesis of  $\text{Ni}(\text{OH})_2$  porous nanoplates.* In a typical synthesis, 30 mg of Ni-Ni PBA nanoplates dissolved in 20 mL of ethanol was first mixed with 10 mL of 2 M NaOH aqueous solution. After magnetic stirring of the mixed solution for 10 minutes, the as-prepared product was collected by several rinse-centrifugation cycles and dried at 70 °C overnight.

*Synthesis of NiO porous nanoplates.* In a typical synthesis, the as-prepared Ni-Ni PBA nanoplates were placed into a porcelain boat and calcined at 300 °C for 1 h with a heating rate of 1 °C  $\text{min}^{-1}$  in air.

*Materials characterization.* The crystal phase of the products was examined by X-ray diffraction (XRD) on a Rigaku D/MAX RINT-2000 X-Ray Diffractometer. Field-emission scanning electron microscope (FESEM; JEOL, JSM07600F) and transmission electron microscope (TEM; JEOL, JEM-

2100F) were used to examine the morphology of the samples. The composition of the samples and elemental mapping was analyzed by energy-dispersive X-ray spectroscopy (EDX) attached to the TEM instrument. X-ray photoelectron spectrometer (XPS, VG microtech ESCA2000) was used for the analysis of the composition of the as-synthesized samples. Fourier transform-infrared spectroscopy (FT-IR) was carried out on a Nicolet 5700 FT-IR Spectrometer. The specific surface area of as-synthesized material was measured on Autosorb-1 at liquid-nitrogen temperature.

*Electrochemical measurements.* The OER and HER activity was evaluated in a three-electrode configuration using a rotating disk electrode (RDE) (Autolab RDE/2, at a rotation speed of 1600 rpm) with an Autolab potentiostat/galvanostat (Model PGSTAT-72637) workstation at ambient temperature. A glassy carbon disk electrode (GCDE) with a diameter of 3 mm was used as the support for the working electrode. The catalyst suspension was prepared by dispersing 3.5 mg of catalyst in 1 mL of solution containing 0.5 mL of DI water, 0.44 mL of ethanol and 60  $\mu\text{L}$  of 0.5 wt.% Nafion solution followed by ultrasonication for 30 min. 4  $\mu\text{L}$  of the catalyst suspension was pipetted onto the GCDE surface using a micropipettor and then dried at ambient temperature. The catalyst loading amount is 0.2  $\text{mg cm}^{-2}$  on the GCDE. A Ag/AgCl (KCl saturated) electrode was used as the reference electrode and a platinum disc electrode was used as the counter electrode. Potentials were referenced to a reversible hydrogen electrode (RHE):  $E(\text{RHE}) = E(\text{Ag/AgCl}) + (0.2 + 0.059 \text{ pH})$ . Linear sweep voltammetry (LSV) was recorded in 1.0 M KOH (pH = 13.62) or 0.5 M  $\text{H}_2\text{SO}_4$  (pH = 0.3) at a scan rate of 5  $\text{mV s}^{-1}$  to obtain the polarization curves. The long-term stability tests were performed by continuous LSV scans. For OER, a sweep rate of 20  $\text{mV s}^{-1}$  was used, while for HER a sweep rate of 50  $\text{mV s}^{-1}$  was used. All the data presented were corrected for  $iR$  losses and background current. EIS was performed at various overpotentials with frequency from 0.1 to 100,000 Hz and an amplitude of 5 mV.

**Table S1.** Comparison of the OER activity for several recently reported active non-metal based electrocatalysts in alkaline solution.

<b>Electrocatalysts</b>	<b>Loading [mg cm<sup>-2</sup>]</b>	<b><math>\eta@10</math> mA cm<sup>-2</sup> [mV]</b>	<b>Tafel slope (mV dec<sup>-1</sup>)</b>	<b>Ref.</b>
Ni-P	0.20	300	64	This work
Ni(OH) <sub>2</sub>	0.20	360	111	This work
NiO	0.20	430	81	This work
Ni <sub>2</sub> P nanoparticles	0.14	290	59	[1]
N <sub>2</sub> P nanowires	0.14	330	47	[1]
Amorphous Ni-Co binary oxide	Not reported	325	39	[2]
$\alpha$ -Ni(OH) <sub>2</sub> hollow spheres	0.20	331	42	[3]
$\beta$ -Ni(OH) <sub>2</sub> nanoplates	0.20	444	111	[3]
Ni-Co oxide hierarchical nanosheets	Not reported	340	51	[4]
Ni-substituted Co <sub>3</sub> O <sub>4</sub> nanowire array	Not reported	~370	65-74	[5]
Ni <sub>x</sub> Co <sub>3-x</sub> O <sub>4</sub> nanowire array	2.3-2.7	~370	59-64	[6]
Co <sub>3</sub> O <sub>4</sub> /N-doped graphene	1.00	310	67	[7]
Nitrogen-doped crumpled graphene-CoO	0.70	340	71	[8]
Co <sub>3</sub> O <sub>4</sub> -carbon porous nanowire arrays	~0.2	290	70	[9]

**Table S2.** Comparison of the HER activity for several recently reported nickel phosphides based electrocatalysts in acid solution.

<b>Electrocatalysts</b>	<b>Loading [mg cm<sup>-2</sup>]</b>	<b><math>\eta@10 \text{ mA cm}^{-2}</math> [mV]</b>	<b>Tafel slope (mV dec<sup>-1</sup>)</b>	<b>Ref.</b>
Ni-P nanoplates/GC	0.20	110	73	This work
Nanostructured Ni <sub>5</sub> P <sub>4</sub> films	3.48	140	40	[10]
Ni <sub>2</sub> P nanorods arrays/Ni foam	Not reported	131	106.1	[11]
N <sub>2</sub> P nanoparticles/GC	0.38	120	87	[12]
N <sub>2</sub> P nanoparticles/Ti	2.00	120	60	[13]
N <sub>2</sub> P nanorods/Ti	0.51	180	76	[14]
Ni <sub>5</sub> P <sub>4</sub> -Ni <sub>2</sub> P-nanosheets array	68.20	120	79.1	[15]
Ni <sub>2</sub> P/carbon nanospheres	0.18	92	46	[16]
Ni <sub>12</sub> P <sub>5</sub> nanoparticles/Ti	3.00	107	63	[17]

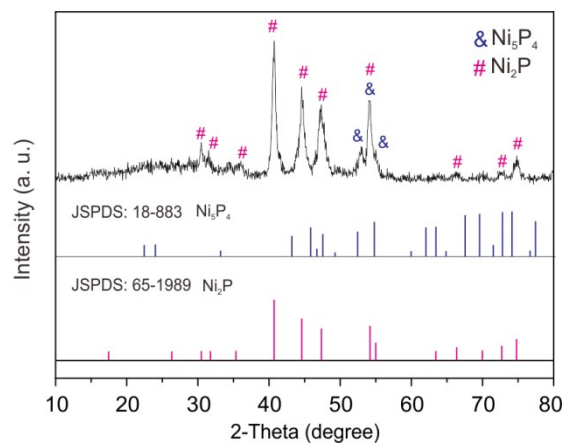
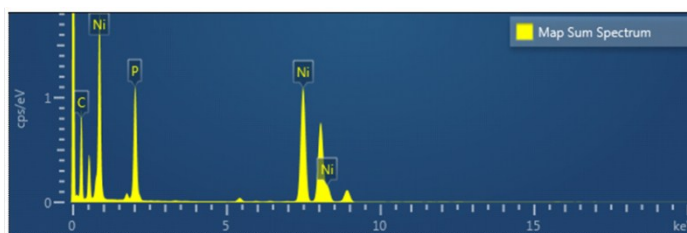


**Fig. S1** XRD pattern of Ni-P porous nanoplates.



Element	Wt%	Atomic %
C	30.88	61.67
P	27.54	21.33
Ni	41.58	16.99
Total:	100.00	100.00

**Fig. S2** EDX spectrum of Ni-P porous nanoplates.

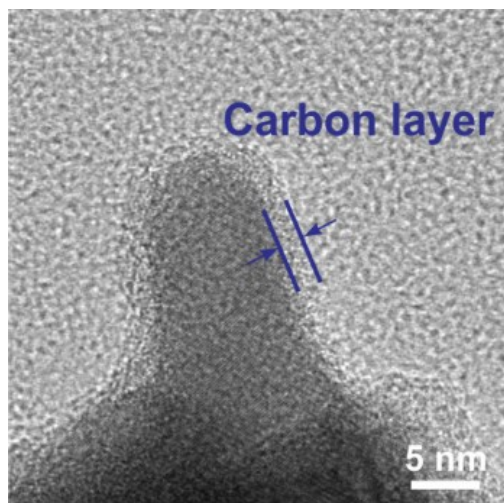


**Fig. S3** HRTEM image of Ni-P porous nanoplates.

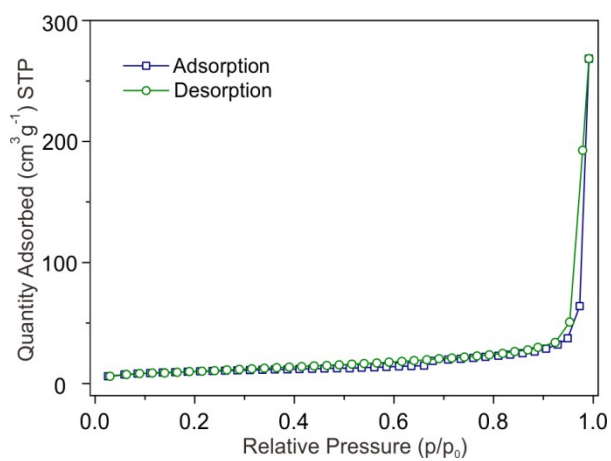


**Fig. S4** N<sub>2</sub> adsorption-desorption isotherm of carbon coated nickel phosphides porous nanoplates.

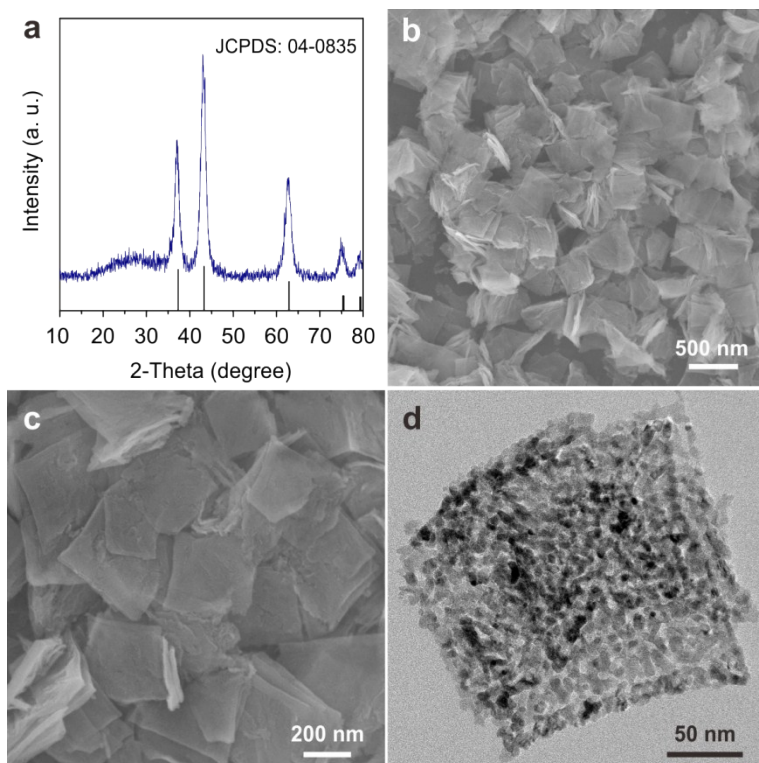


**Fig. S5** XRD pattern (a), FESEM images (b, c), and TEM image (d) of NiO porous nanoplates.



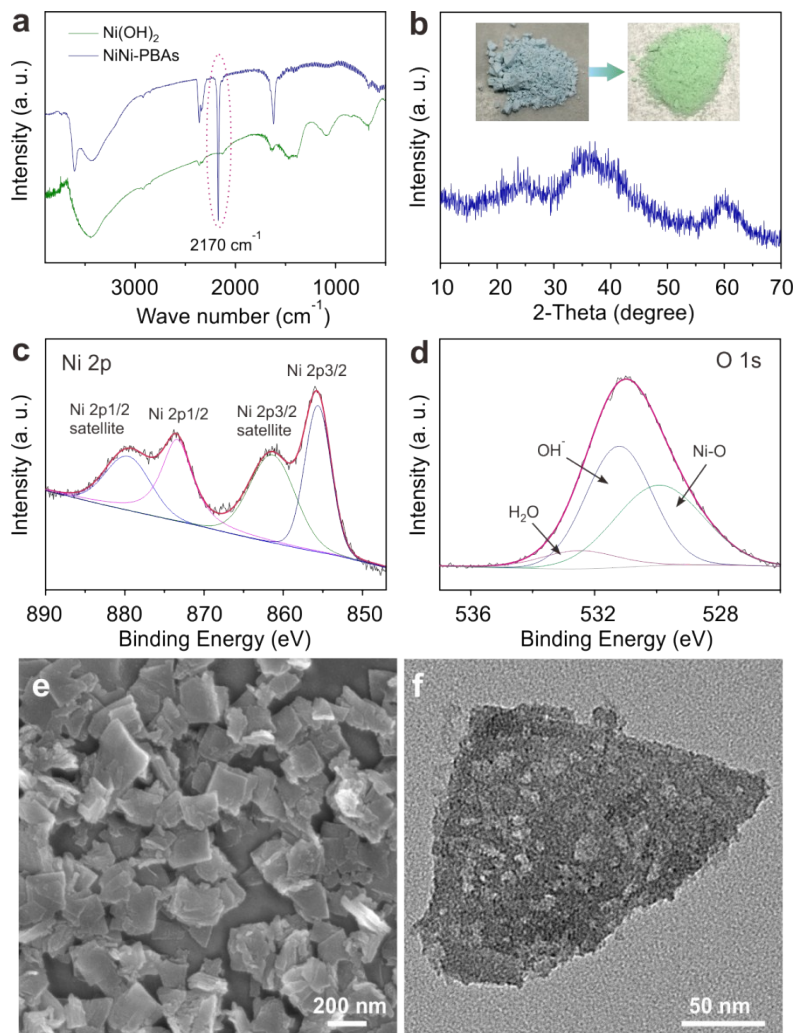


**Fig. S6** (a) FTIR spectra of NiNi-PBA and Ni(OH)<sub>2</sub> nanoplates; (b) XRD pattern; high resolution XPS spectra of Ni 2p (c) and O 1s (d), FESEM image (e), and TEM image (f) of Ni(OH)<sub>2</sub> porous nanoplates.

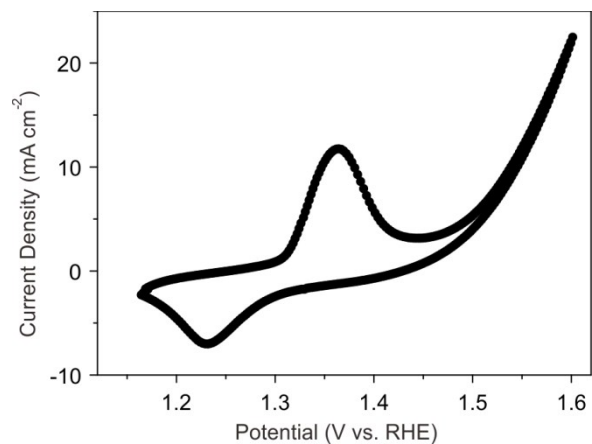


**Fig. S7** Cyclic voltammogram of carbon coated nickel phosphides porous nanoplates in 1.0 M KOH.

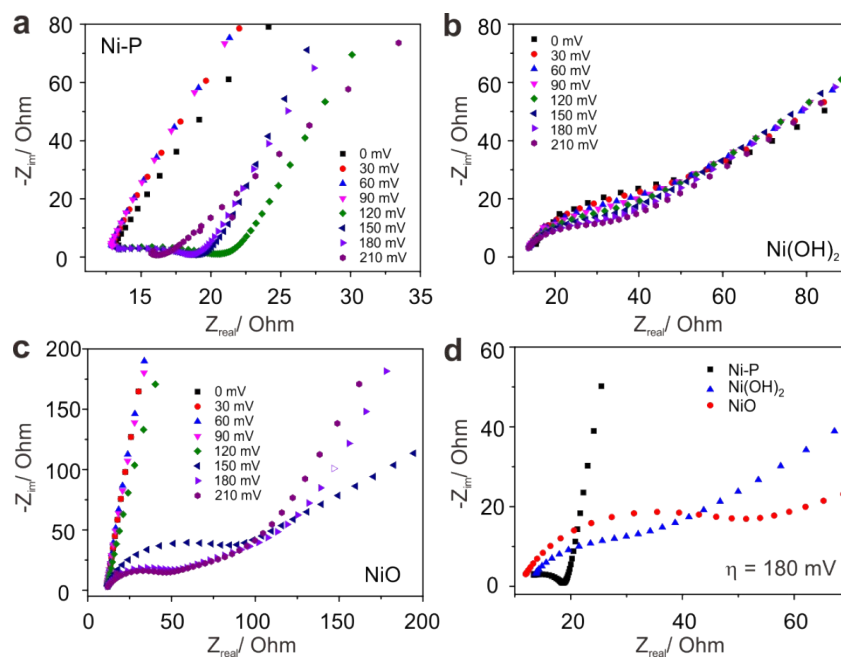


**Fig. S8** EIS Nyquist plots of Ni-P (a), Ni(OH)<sub>2</sub> (b), and NiO porous nanoplates in 1.0 M KOH at various overpotentials; Comparison of Ni-P, Ni(OH)<sub>2</sub>, and NiO porous nanoplates in 1.0 M KOH at a overpotential of 180 mV.

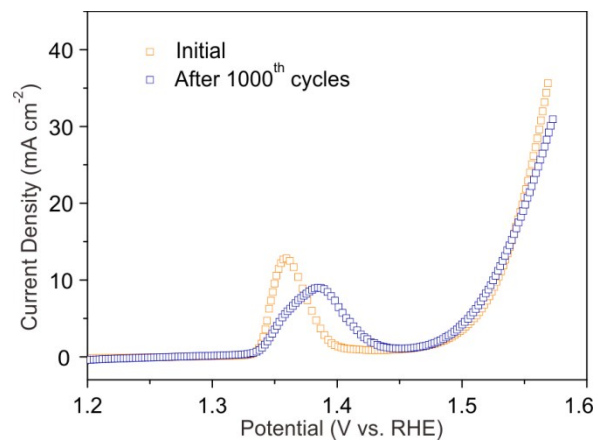


**Fig. S9** Polarization curves after continuous potential sweeps of Ni-P porous nanoplates at  $20 \text{ mV s}^{-1}$  in  $1.0 \text{ M KOH}$ .

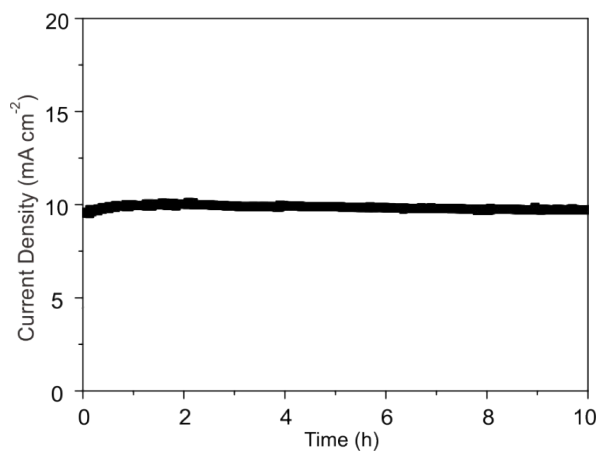


**Fig. S10** Current-time plot of Ni-P electrode with a constant applied potential of  $1.53 \text{ V vs. RHE}$  in  $1.0 \text{ M KOH}$ .

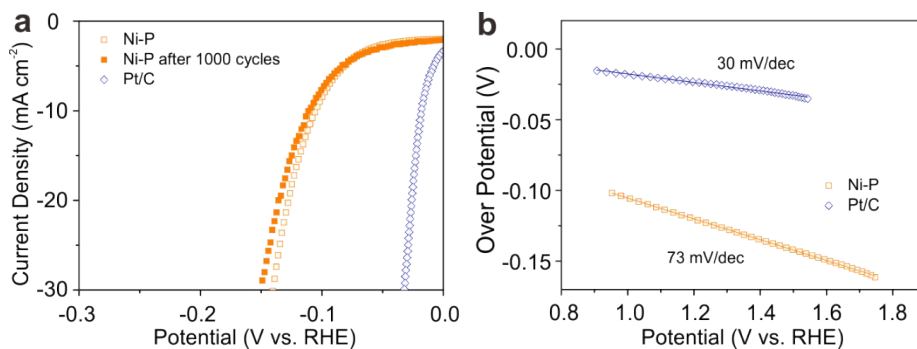


**Fig. S11** HER performance of Ni-P porous nanoplates in 0.5 M H<sub>2</sub>SO<sub>4</sub>: (a) LSV curves and (b) Tafel plots.

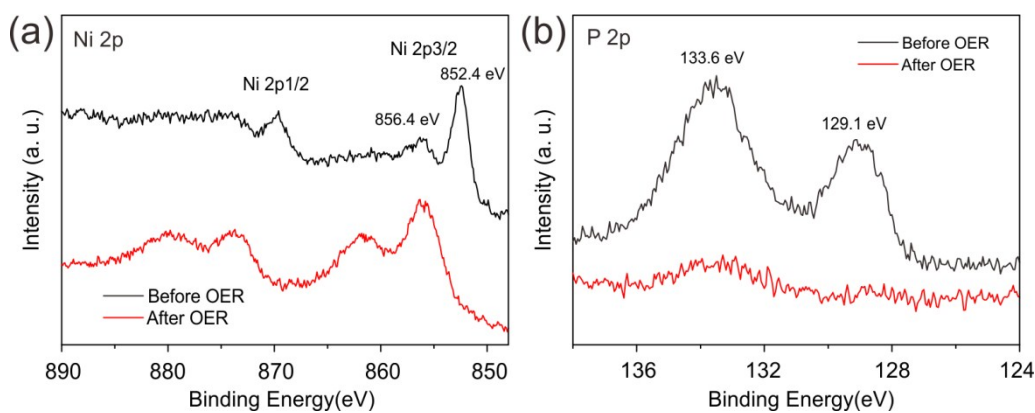


**Fig. S12** High-resolution Ni 2p (a) and P 2p (b) XPS spectra of Ni-P porous nanoplates before and after OER process at a constant applied potential of 1.5 V vs. RHE in 1.0 M KOH for 1 h.

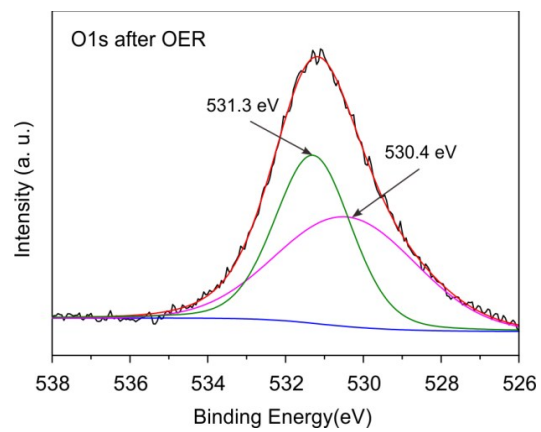


**Fig. S13** High-resolution O1s XPS spectra of Ni-P porous nanoplates after OER process at a constant applied potential of 1.5 V vs. RHE in 1.0 M KOH for 1 h.

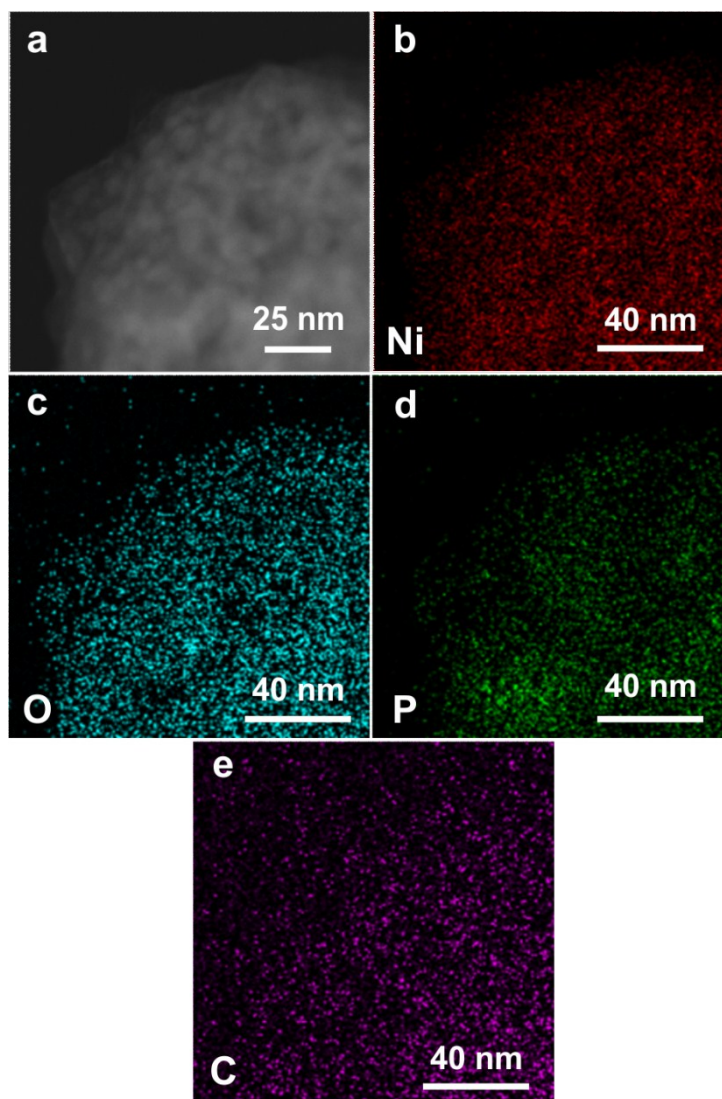


**Fig. S14** TEM image of Ni-P porous nanoplates after OER process at a constant applied potential of 1.5 V vs. RHE in 1.0 M KOH for 1 h (a). (b-e) Corresponding EDX mapping of the elements on the sample region shown in (a). (b) Nickel elemental mapping. (c) Oxygen elemental mapping. (d) Phosphorus elemental mapping. (e) Carbon elemental mapping.

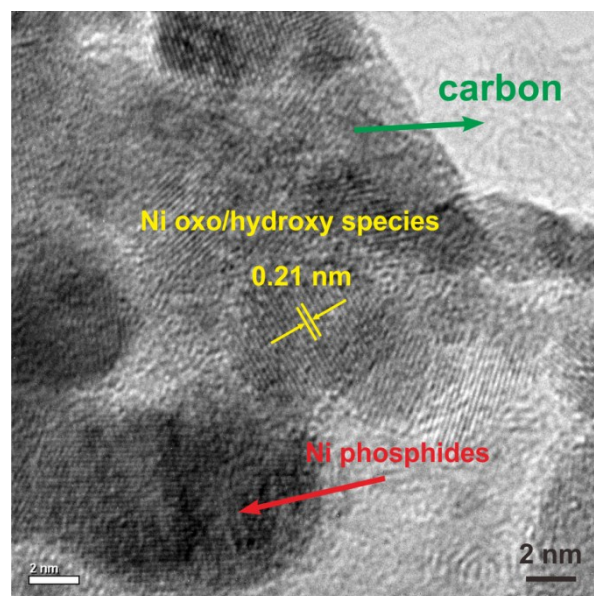


**Fig. S15** High-resolution TEM image of Ni-P porous nanoplates after OER process at a constant applied potential of 1.5 V vs. RHE in 1.0 M KOH for 1 h.

## References

- [1] L. A. Stern, L. G. Feng, F. Song, X. L. Hu, *Energy Environ. Sci.* **2015**, *8*, 2347-2351.
- [2] Y. Yang, H. L. Fei, G. D. Ruan, C. S. Xiang, J. M. Tour, *ACS Nano* **2014**, *8*, 9518-9523.
- [3] M. R. Gao, W. C. Sheng, Z. B. Zhuang, Q. R. Fang, S. Gu, J. Jiang, Y. S. Yan, *J. Am. Chem. Soc.* **2014**, *136*, 7077-7084.
- [4] H. Y. Wang, Y. Y. Hsu, R. Chen, T. S. Chan, H. M. Chen, B. Liu, *Adv. Energy Mater.* **2015**, *5*, 1500091.
- [5] B. A. Lu, D. X. Cao, P. Wang, G. L. Wang, Y. Y. Gao, *Int. J. Hydrogen Energy* **2011**, *36*, 72-78.
- [6] Y. G. Li, P. Hasin, Y. Y. Wu, *Adv. Mater.* **2010**, *22*, 1926-1929.
- [7] Y. Y. Liang, Y. G. Li, H. L. Wang, J. G. Zhou, J. Wang, T. Regier, H. J. Dai, *Nat. Mater.* **2011**, *10*, 780-786.
- [8] S. Mao, Z. H. Wen, T. Z. Huang, Y. Hou, J. H. Chen, *Energy Environ. Sci.* **2014**, *7*, 609-616.
- [9] T. Y. Ma, S. Dai, M. Jaroniec, S. Z. Qiao, *J. Am. Chem. Soc.* **2014**, *136*, 13925-13931.
- [10] M. Ledendecker, S. Krick Calderon, C. Papp, H. P. Steinruck, M. Antonietti, M. Shalom, *Angew. Chem. Int. Ed.* **2015**, DOI: 10.1002/anie.201502438.
- [11] X. G. Wang, Y. V. Kolen'ko, L. F. Liu, *Chem. Commun.* **2015**, *51*, 6738-6741.
- [12] L. G. Feng, H. Vrabel, M. Bensimon, X. L. Hu, *Phys. Chem. Chem. Phys.* **2014**, *16*, 5917-5921.
- [13] Z. H. Pu, Q. Liu, C. Tang, A. M. Asiri, X. P. Sun, *Nanoscale* **2014**, *6*, 11031-11034.
- [14] A. L. Lu, Y. Z. Chen, H. Y. Li, A. Dowd, M. B. Cortie, Q. S. Xie, H. Z. Guo, Q. Q. Qi, D. L. Peng, *Int. J. Hydrogen Energy* **2014**, *39*, 18919-18928.
- [15] X. G. Wang, Y. V. Kolen'ko, X. Q. Bao, K. Kovnir, L. F. Liu, *Angew. Chem. Int. Ed.* **2015**, *54*, 8188-8192.
- [16] Y. Pan, Y. Q. Liu, C. G. Liu, *J. Power Sources* **2015**, *285*, 169-177.
- [17] Z. P. Huang, Z. B. Chen, Z. Z. Chen, C. C. Lv, H. Meng, C. Zhang, *ACS Nano* **2014**, *8*, 8121-8129.